Photo-oxidative damage of photosystem I by repetitive flashes and chilling stress in cucumber leaves

Ginga Shimakawa, Pavel Müller, Chikahiro Miyake, Anja Krieger-Liszkay, Pierre Sétif

Photo-oxidative damage of photosystem I by repetitive flashes and chilling stress in cucumber leaves

Ginga Shimakawa[1,2], Pavel Müller[1], Chikahiro Miyake[2], Anja Krieger-Liszkay[1,*], Pierre Sétif[1]

[1]Université Paris-Saclay, Institute for Integrative Biology of the Cell (I2BC), CEA, CNRS, 91198 Gif-sur-Yvette, France

[2]Graduate School for Agricultural Science, Kobe University, 1-1 Rokkodai, Nada, Kobe 657-8501, Japan

***Corresponding author:** Anja Krieger-Liszkay, e-mail: anja.liszkay@i2bc.paris-saclay.fr

ORCID IDs: 0000-0002-8557-2096 (G.S.); 0000-0002-3245-0810 (P.M.); 0000-0002-6101-4006 (C.M.); 0000-0001-7141-4129 (A.K.-L.); 0000-0002-6101-4006 (P.S.)

Running title: Molecular mechanism of photosystem I photoinhibition

Abstract

Photosystem I (PSI) is an essential protein complex for oxygenic photosynthesis and is also known to be an important source of reactive oxygen species (ROS) in the light. When ROS are generated within PSI, the photosystem can be damaged. The so-called PSI photoinhibition is a lethal event for oxygenic phototrophs, and it is prevented by keeping the reaction center chlorophyll (P700) oxidized in excess light conditions. Whereas regulatory mechanisms for controlling P700 oxidation have been discovered already, the molecular mechanism of PSI photoinhibition is still unclear. Here, we characterized the damage mechanism of PSI photoinhibition by *in vitro* transient absorption and electron paramagnetic resonance (EPR) spectroscopy in isolated PSI from cucumber leaves. Photodamage to PSI was induced by two different light treatments: 1. continuous illumination with high light at low (chilling) temperature (C/LT) and 2. repetitive flashes at room temperature (F/RT). These samples were compared to samples that had been illuminated with high light at room temperature (C/RT). The [Fe-S] clusters F_X and (F_A F_B) were destructed in C/LT but not in F/RT. Transient absorption spectroscopy indicated that half of the charge separation was impaired in F/RT, however, low-temperature EPR revealed the light-induced F_X signal at a similar size as in the case of C/RT. This indicates that the two branches of electron transfer in PSI were affected differently. Electron transfer at the A-branch was inhibited in F/RT and also partially in C/LT, while the B-branch remained active.

Keywords: Photosynthesis; Photosystem I; Photoinhibition; Reactive oxygen species

Introduction

Photosystem I (PSI) is a large protein complex composed of 12−13 subunits, embedded into the thylakoid membrane. PSI catalyzes the light-induced electron transfer from plastocyanin (PC) in the thylakoid lumen to ferredoxin (Fd) in the chloroplast stroma. Light energy absorbed by an antenna system is transferred to the primary electron donor P700 in the reaction center composed of the membrane-spanning PsaA and PsaB subunits. P700 is a dissymmetric dimer of chlorophyll (Chl) molecules, and the singlet photo-excited state (P700*) leads to charge separation, generating $P700^+$ and reduction of the electron acceptors A_0, a Chl *a* molecule, then phylloquinone (PhQ) A_1, and the three [4Fe-4S] clusters F_X, F_A, and F_B until Fd is finally reduced [1,2]. Forward electron transfer is in the picoseconds or tens of picoseconds time range for the initial charge separation between P700 and A_0 and reduction of the PhQs and in the tens or hundreds of nanoseconds time range for oxidation of the reduced PhQ and electron transfer between the [4Fe-4S] clusters. Two branches for the electron transfer from P700 to F_X, the so-called A- and B-branches are active in PSI [3-5], consistent with the similar protein electrostatic environments of PsaA and PsaB [6]. Nevertheless, it should be noted that the electron transfer occurs primarily along the A-branch in PSI [7,8] as the analyses of transient absorption changes suggested that the ratios of the A- and B-branch electron transfers were 95:5 at 77 K and 77:23 at room temperature (298 K) [9].

Since 1970s, PSI has been recognized as the main site for light-induced reduction of O_2 to superoxide anion radical ($O_2^{\bullet-}$), termed as the Mehler reaction [10,11]. Whereas $O_2^{\bullet-}$ generated in the stroma seems to be immediately scavenged by superoxide dismutase (SOD) and the subsequently formed H_2O_2 by ascorbate peroxidases, the one generated within the protein complex or released inside the thylakoid membranes may oxidatively attack the PSI components before being detoxified. Since the midpoint redox potential of the $O_2/O_2^{\bullet-}$ pair in thylakoid membranes is assumed to be around −550 mV [12], PhQs and [4Fe-4S] clusters are thermodynamically plausible as the O_2 photoreduction sites, as demonstrated by [13]. When [4Fe-4S] clusters are kept highly reduced, $O_2^{\bullet-}$ can react with them generating hydroxyl radicals ($^{\bullet}OH$), more deleterious ROS than $O_2^{\bullet-}$ [14]. Overall, PSI carries the potential risk to photo-oxidatively impair itself through ROS generation. Because the protein complex takes days or weeks to recover [15], photoinhibition of PSI can potentially be a lethal event for oxygenic phototrophs.

PSI photoinhibition is rarely observed *in vivo* even in excess light conditions because P700 is kept oxidized by regulatory mechanisms in response to high light and CO_2 limitation to prevent ROS generation. The so-called P700 oxidation is the common physiological response

in oxygenic phototrophs to keep the [4Fe-4S] clusters oxidized [16], which is supported by both the suppression of electron transport into PSI and the electron safety valve at the acceptor side of PSI [17]. Therefore, *in vivo* PSI photoinhibition can occur only in specific situations, where the acceptor side of PSI is strongly reduced with PSII activity being sustained. PSI photoinhibition has been first reported in chilling sensitive plants such as cucumber [18]. The molecular mechanism of "chilling-induced PSI photoinhibition" has been already well characterized, and [4Fe-4S] clusters are the primary damage sites [19]. Simultaneously with the suppression of photosynthetic CO_2 assimilation, the enzyme activities of SOD and peroxidases decline at low temperature in cucumber leaves, allowing $O_2^{\bullet-}$ to directly attack [4Fe-4S] clusters or produce •OH [20,21]. *In vivo* PSI photoinhibition at room temperature has been observed in mutants of plants, algae, and cyanobacteria regulatory mechanisms deficient in P700 oxidation [22-25]. Furthermore, Sejima et al. (2014) have found that repetitive short pulse (rSP) illumination in the dark can easily mimic the situation where the acceptor side of PSI is severely reduced triggering PSI photoinhibition [26]. rSP photoinhibition was reproduced at room temperature in a variety of wild-type plant species [15,27-29], and rSP is regarded as a good tool for studying the molecular mechanism of PSI photoinhibition *in vivo*.

Here, we aimed to elucidate the molecular mechanism of *in vivo* PSI photoinhibition at room temperature using the rSP illumination technique and compared it with chilling-induced PSI photoinhibition in cucumber leaves. Unexpectedly, [4Fe-4S] clusters of PSI were not damaged by rSP illumination at room temperature. Instead, the amplitude of P700 oxidation by single turnover flash was significantly smaller in the treated leaves, suggesting the photo-oxidative damage at an electron acceptor prior to Fx. In PSI photoinhibition at chilling temperatures, impairment of [4Fe-4S] clusters was confirmed but, additionally, the primary acceptors were partially damaged. Based on these data, we concluded that ROS was generated at A_1 leading to its partial damage. Even at chilling temperature, ROS can diffuse and damage [4Fe-4S] clusters.

Materials and Methods

Photoinhibition treatments

Photoinhibition treatments were performed according to previous studies [18,26] with some modifications. Cucumber plants (*Cucumis sativus* L.) were grown on soil in a long-day laboratory growth condition (16 h-light/8 h-dark, 200 μmol photons m^{-2} s^{-1}, white fluorescent lamp, 25°C). The leaves detached from 3−4 week old plants were floated on tap water at 25 ± 2°C or 4 ± 2°C, and then illuminated with continuous light (200 μmol photons m^{-2} s^{-1}, white fluorescent lamp) or rSP (6,000 μmol photons m^{-2} s^{-1}, 800 ms, every 10 s in the dark, blue LED from an Imaging-PAM-MAX/L, Walz, Effeltrich, Germany) (Fig. S1). Before and after the photoinhibition treatments, the amount of total photo-oxidizable P700 (P_m) was determined as described below.

Purification of PSI

PSI was isolated from the treated cucumber leaves starting from thylakoid membranes and using β-dodecyl maltoside as detergent according to the protocol previously reported [30]. The lower band of the sucrose gradient containing PSI was collected, frozen in liquid nitrogen, and stored at −80°C.

In vivo near-infrared absorption spectroscopy

The redox state of P700 was evaluated from *in vivo* near-infrared absorbance [31] with a Dual-PAM-100 (Walz). Pulse-amplitude modulated near-infrared measuring lights (830 and 870 nm) were applied to measure the transmittance of $P700^{\bullet+}$. P_m values were determined by applying a 300-ms saturation flash (8,000 μmol photons m^{-2} s^{-1}) after 4-s illumination with a far-red light (740 nm) at the same position of cucumber leaves before and after photoinhibition treatments.

In vitro flash absorption spectroscopy

$P700^{\bullet+}$ decay kinetics in isolated PSI following a single turnover saturating laser flash was measured at 800 nm in PSI preparations as previously described [32]. Signals at 820 nm were obtained using the following setup: the samples were excited at 600 nm (by laser flashes of ~5.6 mJ cm^{-2} intensity, ~5 ns duration and 0.2 Hz repetition rate) by a Nd:YAG-pumped optical parametric oscillator (Brillant B/Rainbow, Quantel, France). The excitation pulses were attenuated by 1 to 5 neutral density filters of T = 47 % at 600 nm. Continuous measuring light was provided by a laser diode emitting at 819 nm (SDL-5411-G1, Spectra Diode Labs), passed

through a cut-off filter RG780 (to suppress weak contaminations below 750 nm in the emission of the laser diode). The measuring light was perpendicular to the excitation laser beams and passed through the sample along the 10 mm path of a 2 × 2 × 10 mm (width × height × length) quartz cell with self-masking solid black walls (from Starna). Flash-induced changes of the transmission of the sample were monitored behind the sample and an 820 nm interference filter (to suppress stray light and the fluorescence induced by the excitation flash) by a Si photodiode (Alphalas UPD-500; rise time, ~500 ps; sensitive area, 0.5 mm^2) coupled to a digital oscilloscope (Tektronix MSO64; bandwidth limit set to 6 GHz and the sampling rate to 1.25 Gsamples s^{-1}). Kinetic traces shown in Fig. 3 and Fig. S5 are averages of 32 signals.

Measurements were done in 20 mM Tricine (pH 8), 125 mM sucrose, 5 mM $MgCl_2$, 30 mM NaCl, 0.5 mM ascorbate and 5 µM dichlorphenolindiphenol (DCPIP). The $P700^{\bullet+}$ decay kinetics were reasonably fitted with two exponential components, from which the rates k_r and k_e of recombination and electron escape from the terminal electron acceptor (F_A, F_B) were determined as explained in Mignée et al. (2017). In the case of single electron turnover, i.e. without accumulation of reduced acceptors, escape to O_2 notably occurs mostly if not exclusively from (F_A, F_B) as shown by the fact that binding of an inactive gallium-substituted Fd to PSI greatly inhibits electron escape [33].

Low-temperature EPR spectroscopy

Continuous wave EPR spectra were recorded with a Bruker ER 200D X-band spectrometer equipped with an Oxford Instruments cryostat. The microwave frequency was measured with a microwave frequency counter HP 5350B. Samples were prepared in calibrated tubes of 3-mm internal diameter. Most samples were prepared in Tricine 20 mM pH 8.0, 125 mM sucrose, 5 mM $MgCl_2$, 30 mM NaCl. When indicated, 2 mM ascorbate and 30 µM DCPIP were added to the samples. In case of dithionite, a solution of 5 mM dithionite at pH 8.0 and as redox mediators methyl viologen and triquat were added and the sample was illuminated at room temperature for 1 min at weak white light intensity and frozen into liquid nitrogen under ambient light conditions. Illumination of EPR tubes at 200 K was performed with a tungsten–halogen lamp (white light intensity of 200 mW cm^{-2}) in a nitrogen gas flow system (Bruker, B-VT-3000). Light-induced warming of the tubes was minimized by filtering the light with a water cuvette and an infrared absorbing filter. The following procedure was followed for illumination at 200 K: samples were transferred in room light from liquid nitrogen to the gas flow system, kept in room light for 1 min for temperature equilibration, illuminated for a given time period, then cooled down to 120 K within the gas flow system before being transferred to liquid

nitrogen for later EPR measurements.

Results

Photoinhibition of PSI in cucumber leaves at room and low temperatures

PSI purified from cucumber leaves was submitted to three different illumination treatments for 4−5 hours: continuous light at room temperature (25 ± 2°C), continuous light at low temperature (4 ± 2°C), and repetitive flashes in the dark at room temperature. Before and after treatments, the maximum signal of $P700^+$ absorption, labelled as P_m, was measured. P_m was not affected by the continuous light treatment at room temperature, while both other treatments, i.e., continuous light at low temperature and rSP illumination at room temperature, led to a decrease in P_m by 45% and 33%, respectively (Table 1). In the following, the corresponding PSI samples will be referred to as C/RT, C/LT and F/RT, respectively (C for continuous, F for repetitive flashes, RT for room temperature, and LT for low temperature; Fig. S1). The absorption spectra of these three different PSI are superimposable (Fig. S2). This supports the idea that their antenna size is identical and that there is no significant differential bleaching of antenna pigments caused by the different treatments. These three PSI samples were studied by EPR for the quantification of [4Fe-4S] clusters and by flash-absorption spectroscopy in the near infra-red for measuring the kinetics of $P700^+$ (and sometimes $^3P700$ and Chl antenna triplet states) formation and decay. For most of the EPR and all absorption measurements, the PSI properties were measured at similar, i.e., within 20%, Chl concentrations and, except when specifically indicated, data will be shown after normalizing the kinetics or spectra to same Chl concentrations, to allow direct comparisons.

Quantitation of [4Fe-4S] clusters by EPR spectroscopy

EPR spectra of the three types of PSI were recorded for measuring both the content and the low-temperature light-induced reduction of the [4Fe-4S] clusters. For measuring the content, the clusters were initially reduced in darkness by adding sodium dithionite at pH 10 in the presence of low-potential redox mediators. As this led to incomplete (F_A F_B) reduction, the EPR tubes were then illuminated at 200 K for successive periods until the maximal extent of F_X reduction was observed. The resulting spectra are shown in Fig. 1 where the characteristic EPR lines of $(F_A\ F_B)_{2red}$ (g = 1.89, 1.925, 1.945, and 2.05) and F_{Xred} (indicated by asterisks) are observed under conditions, which are optimal for F_X detection. Whereas the EPR spectra of C/RT and F/RT are rather similar, the C/LT spectrum is significantly smaller than those of the two other samples. From the most easily observable high-field peak of F_{xred} at g = 1.77, one may estimate that C/LT contains only about 30−40% F_X as compared to C/RT and F/RT (Fig.

1A). This estimation is very crude because of the large underlying baseline present under these conditions of low temperature and high microwave power. Whereas the F_{Xred} signals are quasi-identical in C/RT and F/RT samples, a comparison between $(F_A\ F_B)_{2red}$ signals is not precise under the conditions of Fig. 1A due to the fact that these signals are highly saturated and strongly depend on temperature. Much better conditions for comparing $(F_A\ F_B)_{2red}$ at 25 K with non-saturating microwave power were used in Fig. 1C. Under these conditions, the signals are quasi-identical in C/RT and F/RT whereas the $(F_A\ F_B)$ content in C/LT is about 70% of that in C/RT.

In addition to PSI reduced by dithionite, light-induced signals were measured in samples containing ascorbate and DCPIP as electron donors. At low temperature, PSI illumination leads to some irreversible charge separation between P700 and $(F_A\ F_B)$ in part of the reaction centers. The $(F_A\ F_B)_{1red}$ signals resulting from this process are shown in Fig. 2B and D for the three types of PSI. In Fig. 1B, the signals are shown at 15 K with a saturating microwave power. For quantitative spin measurements, the same data are also shown at higher temperature (25 K) and non-saturating microwave power conditions (Fig. 1D). The comparison between the different PSI samples gives similar conclusions to those for the dithionite samples: the C/RT and F/RT $(F_A\ F_B)_{1red}$ signals are very similar whereas the signal is smaller for C/LT.

The spin amounts due to $(F_A\ F_B)$ signals can be compared between Fig. 1C and D (Table 2), for which the EPR conditions including non-saturating microwave power were the same. Moreover, it can be noted that F_X is no longer visible at 25 K, as it is widely broadened due to extremely fast spin-lattice relaxation [34], so that it minimally interferes with the quantitation of $(F_A\ F_B)_{2red}$ spins. The spin quantitation is in accordance with the above conclusions: from the $(F_A\ F_B)_{2red}$ signals, it appears that the $(F_A\ F_B)$ content in F/RT is similar to that of C/RT, whereas it is 70% in C/LT. The efficiency of low temperature charge separation appears to be slightly less in F/RT than in C/RT whereas it is lower in C/LT, especially when normalizing its amount against Chl (i.e., PSI).

Flash-induced measurements at 800 nm with microsecond time resolution

Fig. 2 shows the flash-induced absorption changes measured at 800 nm after excitation by a 700-nm single turnover laser flash. In Fig. 2A, the 100% laser intensity (~25 mJ cm^{-2}) is saturating PSI photochemistry, as judged by the observation that the absorption changes after 50 µs are diminished by less than 5% with a 2-fold decrease in energy (Fig. S3). The most striking observation is the difference in the initial signal amplitudes, being much smaller for both C/LT and F/RT. By comparison to C/RT, the signal is about 50% in F/RT for both the signal

recorded at 3% laser intensity (~0.8 mJ cm^{-2}) and the decay after 50 µs for the 100% laser intensity (i.e., disregarding the antenna triplet signal, see below). Assuming that C/RT is fully active, this reveals that a stable charge separation occurs in only 50% of PSI in F/RT. Moreover, there is no indication that in F/RT forward electron transfer is significantly blocked at the level of the primary Chl acceptor A_0, as such a blockage should give a large signal of ^{3}P700, which would result from a recombination reaction between $P700^+$ and A_0^- in the nanosecond time range [2].

A fast component ($t_{1/2}$ = 7−10 µs) is observable in all three PSI (Fig. 2A). The relative amplitude of this component decreases at lower laser intensities (Fig. S3) so that part or all of it can be attributed to the decay of Chl antenna triplet states. This behavior is also illustrated in Fig. 2B, where the laser intensity is only 3% of that in Fig. 2A. Under these conditions, the amplitudes of the slow phases are *ca.* 50% those observed at 100% laser intensity. No fast microsecond component is observable for both C/RT and F/RT whereas some is still observable in C/LT (Fig. 2B). The spectrum of the 7−10 µs component was studied between 730 and 970 nm. It exhibits features, which are clearly different from those of the slow phases. It is attributed to the decay of ^{3}P700, whereas the slow phases are due to $P700^+$ decay (Fig. S4). In fact, a more precise analysis of the signals recorded at low laser intensity with several exponential decay components shows indeed the presence of a very minor component which could be due to ^{3}P700 (4% of the total decay) whereas about 8% of the decay occurs in the submillisecond time range ($t_{1/2}$ = 530 µs; Table 3). The latter component can be attributed to a recombination reaction between $P700^+$ and secondary acceptors (most probably F_X) when the terminal acceptor (F_A F_B) is destroyed. In C/LT, a similar proportion (9%) of the decay occurs in the submillisecond time range. Its halftime of 180 µs shows, in accordance with the EPR data, that F_X also is partially destroyed so that recombination occurs from a reduced PhQ (Table 3). The ^{3}P700 signal in C/LT is of larger amplitude (24% of the total) than the submillisecond component. The proportion of slow decay indicative of the presence of functional (F_A F_B) is lower in C/LT than in F/RT (38% *vs.* 47%). Very similar proportions are found when comparing the slow phases amplitudes in the different PSI under conditions of saturating laser flashes (Table 3).

Flash-induced measurements at 820 nm with nanosecond time resolution

Some $P700^+$ signal is "missing" when studying the flash-absorption changes with microsecond time resolution. We hence performed measurements at 820 nm on a setup with a much higher time resolution (~5 ns, limited only by the length of the excitation pulse) and in order to find whether this missing part can be "recovered" in case it corresponds to fast sub-microsecond

recombination reactions.[1] As above with the flash-induced measurements at 800 nm, we performed absorption measurements at different laser intensities. With a laser intensity saturating PSI photochemistry, large signals in the microsecond time range were observed in C/RT, which are presumably due to the decay of antenna Chl triplet states. When decreasing the intensity about 20 times, charge separation occurred in about half C/RT. Under these conditions, some microsecond decay is still present, in contrast to the measurements at 800 nm (Fig. S5). This difference is most probably due to the use of different excitation wavelengths (600 nm *vs.* 700 nm for measurements at 820 and 800 nm, respectively) or a possible inhomogeneity of the excitation laser beam (higher light intensity in the center of the sample cell and lower at the edges). Moreover, a large decay with a halftime of about 7 ns was also present at low-intensity excitation. In order to be able to compare the fast absorption decays due to photochemistry in the different PSIs, it is desirable to get rid of antenna signals. As these signals cannot be eliminated by low intensity excitation, we subtracted the C/RT antenna signals from the decays of all 3 PSIs before comparison, as described in detail in Fig. S4. This subtraction procedure assumes that the antenna signals are identical in the different PSIs.

The resulting kinetic traces are shown in Fig. 3 on two different timescales. The resulting trace for C/RT is not decaying in the given time, and almost the same is observed for the decay for F/RT, with only a very minor decay of ~60 ns halftime and no microsecond decay. The missing initial $P700^+$ signal in C/LT and F/RT can therefore be attributed to a lack of primary charge separation leading to A_0 reduction. In contrast with F/RT and C/RT, decay components with significant amplitudes can be observed in C/LT, with a decay of 50 ns halftime followed by a microsecond decay, which is best-fitted with 2 exponential components of 1.4 and 8.1 µs halftimes (Table 4). Two main features should be noted with regard to this kinetic analysis: first, the initial signal amplitude is smaller than that in C/RT, meaning that there is some missing $P700^+$ signal; second, the amplitude of the nanosecond decay is smaller than that of the triplet decay. This observation is opposite to what is expected if the nanosecond decay would correspond mostly to a recombination reaction between $P700^+$ and A_0^- producing $^3P700$ with a 30−50% yield, because the absorption coefficients of the 3 species $P700^+$, $^3P700$ and A_0^- should be rather similar at 820 nm.

Double-flash experiments at 800 nm

[1]Note that the C/LT preparation studied here is slightly different from the one studied for absorption changes at 800 nm and for EPR but is the one used for measuring the $^3P700$ spectrum (Fig. S4). It was selected for the present measurements as it exhibited a larger $^3P700$ signal and potentially a larger nanosecond signal.

At first sight, the fact that upon illumination with continuous light the efficiency of charge separation between P700 and (F_A F_B) at low temperature is almost the same in F/RT as in C/RT (see EPR results, Fig. 1D) appears to contradict the observation that a large part of $P700^+$ is missing in F/RT after a single laser flash (Fig. 2B and 3). This apparent contradiction may be explained by the fact that the photo-accumulation of $(F_A\ F_B)_{1red}$ at low temperature results from numerous successive charge separations. Therefore, we investigated the possibility that a larger proportion of F/RT could undergo charge separation under multiple turnover conditions. This was tested in double flash experiments at 800 nm in the presence of the electron acceptor methyl viologen to avoid recombination reaction involving $(F_A\ F_B)_{1red}$. The results of these experiments are shown for the three PSIs in Fig. 4 and are summarized in Table 5. The two laser flashes were separated by 200 ms and only the slowly decaying part of $P700^+$ is shown. The second-flash increment is larger in F/RT than in C/RT (8% vs 3%) and is even larger in C/LT (12%).

The increment that is observed for F/RT and C/LT, which is larger than for C/RT, suggests that with both photoinhibition treatments, part of PSI which did not undergo charge separation after the first flash was prone to charge separation after the second flash. This observation would suggest a competition of charge separation with unproductive de-excitation pathway(s), resulting in a quantum yield of charge separation lower than one. However, a simple competition mechanism is expected to give a larger signal increment on the second flash: e.g., assuming a yield of charge separation of 0.5, resulting in 50% $P700^+$ formation on the first flash, one would expect a second-flash increment of 25% and a 12.5% third-flash increment, etc... The competition process was further investigated by using a series of 18 saturating 50 µs flashes separated by 2 ms time intervals. The slowly decaying $P700^+$ increased by 7, 18 and 27% after 18 flashes vs the first flash signal for C/RT, F/RT and C/LT. The lower-than-expected signal increase compared to the missing first-flash $P700^+$ signal points to an inhomogeneity in the treated PSIs, i.e., presence of fractions with unequal extent of damage.

Discussion

Mechanism leading to PSI photoinhibition should be elucidated on a molecular level to understand better the potential risk for plants exposed to abiotic stress. In this study, we analyzed PSI purified from cucumber leaves exposed to three types of photoinhibition treatments: continuous light at room temperature, continuous light at chilling temperature, and repetitive flashes in the dark at room temperature (Table 1). Both EPR and flash absorption spectroscopy measurements indicated that the [4Fe-4S] clusters were damaged in C/LT (Fig. 1 and 2), which is consistent with the previous report [19], while the [4Fe-4S] remained intact in the two other samples.

There seems to be a notable contradiction between EPR and flash absorption spectroscopy results, especially in F/RT: i.e., about a half of the charge separation was impaired in flash absorption kinetics at room temperature (Fig. 2) while the amplitudes of the light-induced [4Fe-4S] clusters were the same as those in C/RT in EPR at low temperature (Fig. 1). This contradiction can be explained by the temperature dependency of the two electron transfer branches in PSI as follows. The reaction center core of PSI composed of PsaA and PsaB contains six Chls and two PhQs to drive A- and B-branches from P700 to F_X (Fig. 5). The six Chls are close enough to undergo significant excitonic interactions and suggested to be directly related to the occurrence of charge separation (Srinivasan and Golbeck, 2009) although it is still unknown whether P700 or another Chl are involved in the primary charge separation. The kinetics of PhQ_{red} re-oxidation by (F_A F_B) are in general described as biphasic or even triphasic, involving PhQ_{Ared}, PhQ_{Bred}, and $(F_X\text{-}PhQ_A)_{1red}$ (Srinivasan and Golbeck, 2009). Re-oxidation of PhQ_{B1red} is almost activationless whereas PhQ_{A1red} re-oxidation is strongly activated and becomes blocked at around 200 K: i.e., PhQ_{A1red} does not reduce F_X and recombines with $P700^+$ (Srinivasan and Golbeck, 2009). As a consequence, (F_A F_B) is reduced at low temperature only *via* the B-branch. The quantum yield of this reaction is rather small (about 10%, most probably *via* unfavorable competition with A-branch charge separation) but prolonged illumination at low temperature leads to a large extent of $(F_A\ F_B)_{1red}$ formation (40−80%). These low temperature measurements argue for a competition between these two branches although the details are still unknown. Overall, it could be reasonable that the [4Fe-4S] clusters were reduced without any problems at low temperature (Fig. 1) and the charge separation was impaired at room temperature (Fig. 2) in the situations where the A-branch was damaged in PSI. With this interpretation, the molecular mechanisms of PSI photodamage in C/LT and F/RT are summarized respectively as follows.

In F/RT, [4Fe-4S] clusters are totally intact and as light-reducible as in C/RT at 8−25 K (Fig. 1), which suggests that B-branch is highly active and presumably intact after the treatment with rSP illumination. Additionally, P700 is possibly completely intact. Meanwhile, in flash excitation at room temperature, there must be inactivation of the A-branch leading to about 50% of full charge separation (Fig. 2). Nanosecond (> 10 ns) or microsecond recombination reaction indicated no (or very little) ^{3}P700 formation in F/RT (Fig. 3). Compared to the 50% inactivation of PSI (Fig. 2), the percentage of intact P700 (at least 65% and possibly 100%; Fig. 1) is significantly larger. This suggests that the damage to the A-branch concerns either Chl B2 or Chl A3 and not primarily P700 (Fig. 5). Multiple flashes at room temperature resulted only in a moderate increase in $P700^+$ amplitude, which suggests that in the A-branch degraded PSI there is rather limited redirection of charge separation to the B-branch. In other words, a half charge separation means that in the other 50%, excitation is lost without the possibility to use the B-branch in F/RT. Possibly, several excited and charge-separated states involving the six Chl are quasi-isoenergetic, and an A-branch charge-separated state relaxes by very fast recombination to the ground state (e.g., between $P700^+$ and Chl $B2^-$). The recent study has shown that the reducible [Fe-S] level decreases during rSP illumination at room temperature in the Arabidopsis wild type plants [16], which is possibly due to the damage at the A-branch. The mechanism of the *in vivo* photodamage to Chl B2 and/or Chl A3 are still unclear, but the ROS generation site should be close to the damage site. One would assume that $O_2^{\bullet-}$ generated by PhQ_{Ared} is the primary cause of PSI photoinhibition *in planta* as reported *in vitro* [13].

In C/LT, 30% of (F_A F_B) was destructed as shown in low temperature EPR signals (Fig. 1). A larger decrease in $(F_A\ F_B)_{1red}$ than in $(F_A\ F_B)_{2red}$ implied a larger loss of F_X rather than (F_A F_B). Although its formation mechanism is not clear, ^{3}P700 is observed in C/LT (Fig. 2). It has been reported that ^{3}P700 is formed from a pair ($P700^+$ PhQ^-) under highly reducing conditions with all three [4Fe-4S] clusters pre-reduced [35]. This process involves singlet-triplet mixing followed by uphill population to the ($P700^+$ Chl A_0^-) radical pair which decays with a high rate/probability to ^{3}P700. Therefore, it exhibits a large activation energy, presumably corresponding to the energy difference between the two pairs ($P700^+$ PhQ^-) and ($P700^+$ Chl A_0^-). As the energy gap is smaller with PhQ_B, it can be proposed that the B-branch quinone is presently involved in the process and that it occurs when F_X is damaged. The observation of PSI photodamage in C/LT was similar to that reported previously [19] except that the charge separation of P700 was also inhibited like in F/RT (Fig. 2). A recent study analyzed both EPR and flash absorption spectroscopy in PSI isolated, after a high light treatment, from *Arabidopsis* leaves of the wild type and the mutant deficient in PGR5, a molecular component important for

keeping P700 oxidized. The mutant PSI damaged at room temperature showed the decrease both in the flash-induced $P700^+$ amplitude and in the EPR signals for the [4Fe-4S] clusters [36], which is similar to the case at C/LT in this study.

Finally, based on the experimental evidence reported so far, ROS leading to PSI photoinhibition are generated within PSI probably close to the reaction center core, and they damage the A-branch of the primary reaction (either Chl B2 or Chl A3) and the [4Fe-4S] clusters. The level of photoinhibition seems to be related to the degrees of the PSI acceptor-side limitation and ROS scavenging capacity. There is no doubt that the ROS generation within PSI is triggered by the excess electron donation into PSI when the acceptor side capacity is low. This shows the physiological importance of regulatory mechanism that keep P700 oxidized in excess light conditions [37].

Author contributions: G.S. and A.K.-L. worked on *in vivo* analyses and isolated photosystem I with assistance from C.M.; P.S., P.M., G.S., and A.K.-L performed transient absorption and EPR spectroscopy; all authors wrote the manuscript.

Funding information: This work benefited from the support of the LabEx Saclay Plant Sciences-SPS (ANR-17-EUR-0007) and the French Infrastructure for Integrated Structural Biology (ANR-10-INBS-05), and was also partially supported by a grant from the Agence Nationale de la Recherche (RECYFUEL project ANR-16-CE05-0026). G.S. was supported by a JSPS oversea research fellowship (201860126). C.M. was supported by Core Research for Evolutional Science and Technology of Japan Science and Technology Agency, Japan (JPMJCR1503).

Conflict of interest: The authors have no conflict of interest to declare.

References

[1] P. Fromme, P. Jordan, N. Krauß, Structure of photosystem I, Biochim. Biophys. Acta Bioenerg. 1507 (2001) 5-31.

[2] K. Brettel, W. Leibl, Electron transfer in photosystem I, Biochim. Biophys. Acta Bioenerg. 1507 (2001) 100-114.

[3] M. Guergova-Kuras, B. Boudreaux, A. Joliot, P. Joliot, K. Redding, Evidence for two active branches for electron transfer in photosystem I, Proc. Natl. Acad. Sci. U.S.A. 98 (2001) 4437-4442.

[4] I. Muhiuddin, P. Heathcote, S. Carter, S. Purton, S. Rigby, M. Evans, Evidence from time resolved studies of the P700+/A1− radical pair for photosynthetic electron transfer on both the PsaA and PsaB branches of the photosystem I reaction centre, FEBS Lett. 503 (2001) 56-60.

[5] V. Ramesh, K. Gibasiewicz, S. Lin, S.E. Bingham, A.N. Webber, Bidirectional electron transfer in photosystem I: accumulation of A_0-in A-side or B-side mutants of the axial ligand to chlorophyll A_0, Biochemistry 43 (2004) 1369-1375.

[6] K. Kawashima, H. Ishikita, Energetic insights into two electron transfer pathways in light-driven energy-converting enzymes, Chem. Sci. 9 (2018) 4083-4092.

[7] F. Yang, G. Shen, W.M. Schluchter, B.L. Zybailov, A.O. Ganago, I.R. Vassiliev, D.A. Bryant, J.H. Golbeck, Deletion of the PsaF polypeptide modifies the environment of the redox-active phylloquinone (A_1). Evidence for unidirectionality of electron transfer in photosystem I, J. Phys. Chem. B 102 (1998) 8288-8299.

[8] W. Xu, P.R. Chitnis, A. Valieva, A. Van der Est, K. Brettel, M. Guergova-Kuras, Y.N. Pushkar, S.G. Zech, D. Stehlik, G. Shen, Electron transfer in cyanobacterial photosystem I: II. Determination of forward electron transfer rates of site-directed mutants in a putative electron transfer pathway from A_0 through A_1 to F_X, J. Biol. Chem. 278 (2003) 27876-27887.

[9] H. Makita, G. Hastings, Directionality of electron transfer in cyanobacterial photosystem I at 298 and 77 K, FEBS Lett. 589 (2015) 1412-1417.

[10] K. Asada, M. Takahashi, Production and scavenging of active oxygen in photosynthesis, in: D.J. Kyle, C.B. Osborne, C.J. Arntzen (Eds.) Photoinhibition, Elsevier, Place Published, 1987, pp. 227-287.

[11] K. Asada, The water-water cycle as alternative photon and electron sinks, Philos Trans R Soc Lond B Biol Sci 355 (2000) 1419-1431.

[12] P. Wardman, Bioreductive activation of quinones: Redox properties and thiol reactivity, Free Radical Res. Commun. 8 (1990) 219-229.

[13] M. Kozuleva, A. Petrova, Y. Milrad, A. Semenov, B. Ivanov, K.E. Redding, I. Yacoby, Phylloquinone is the principal Mehler reaction site within photosystem I in high light, Plant Physiol. 186 (2021) 1848-1858.
[14] B.L. Upham, L.S. Jahnke, Photooxidative reactions in chloroplast thylakoids. Evidence for a Fenton-type reaction promoted by superoxide or ascorbate, Photosynth. Res. 8 (1986) 235-247.
[15] M. Zivcak, M. Brestic, K. Kunderlikova, O. Sytar, S.I. Allakhverdiev, Repetitive light pulse-induced photoinhibition of photosystem I severely affects CO_2 assimilation and photoprotection in wheat leaves, Photosynth. Res. 126 (2015) 449-463.
[16] R. Furutani, S. Wada, K. Ifuku, S. Maekawa, C. Miyake, Higher reduced state of Fe/S-signals, with the suppressed oxidation of P700, causes PSI inactivation in *Arabidopsis thaliana*, Antioxidants 12 (2023) 21.
[17] G. Shimakawa, C. Miyake, Oxidation of P700 ensures robust photosynthesis, Front. Plant Sci. 9 (2018) 1617.
[18] I. Terashima, S. Funayama, K. Sonoike, The site of photoinhibition in leaves of *Cucumis sativus* L. at low temperatures is photosystem I, not photosystem II, Planta 193 (1994) 300-306.
[19] K. Sonoike, I. Terashima, M. Iwaki, S. Itoh, Destruction of photosystem I iron-sulfur centers in leaves of Cucumis sativus L. by weak illumination at chilling temperatures, FEBS Lett. 362 (1995) 235-238.
[20] I. Terashima, K. Noguchi, T. Itoh-Nemoto, Y.-M. Park, A. Kuhn, K. Tanaka, The cause of PSI photoinhibition at low temperatures in leaves of Cucumis sativus, a chilling-sensitive plant, Physiol. Plant. 103 (1998) 295-303.
[21] K. Sonoike, Photoinhibition of photosystem I, Physiol. Plant. 142 (2011) 56-64.
[22] Y. Munekage, M. Hojo, J. Meurer, T. Endo, M. Tasaka, T. Shikanai, PGR5 is involved in cyclic electron flow around photosystem i and is essential for photoprotection in Arabidopsis, Cell 110 (2002) 361-371.
[23] M. Suorsa, F. Rossi, L. Tadini, M. Labs, M. Colombo, P. Jahns, Martin M. Kater, D. Leister, G. Finazzi, E.-M. Aro, R. Barbato, P. Pesaresi, PGR5-PGRL1-dependent cyclic electron transport modulates linear electron transport rate in *Arabidopsis thaliana*, Mol. Plant 9 (2016) 271-288.
[24] Y. Allahverdiyeva, H. Mustila, M. Ermakova, L. Bersanini, P. Richaud, G. Ajlani, N. Battchikova, L. Cournac, E.M. Aro, Flavodiiron proteins Flv1 and Flv3 enable cyanobacterial growth and photosynthesis under fluctuating light, Proc. Natl. Acad. Sci. U.S.A. 110 (2013) 4111-4116.

490 [25] G. Shimakawa, K. Shaku, C. Miyake, Oxidation of P700 in photosystem I is essential for
491 the growth of cyanobacteria, Plant Physiol. 172 (2016) 1443-1450.
492 [26] T. Sejima, D. Takagi, H. Fukayama, A. Makino, C. Miyake, Repetitive short-pulse light
493 mainly inactivates photosystem I in sunflower leaves, Plant Cell Physiol. 55 (2014) 1184-1193.
494 [27] M. Tikkanen, S. Grebe, Switching off photoprotection of photosystem I – a novel tool for
495 gradual PSI photoinhibition, Physiol. Plant. 162 (2018) 156-161.
496 [28] Y.-J. Yang, S.-B. Zhang, J.-H. Wang, W. Huang, Photosynthetic regulation under
497 fluctuating light in field-grown *Cerasus cerasoides*: A comparison of young and mature leaves,
498 Biochim. Biophys. Acta Bioenerg. 1860 (2019) 148073.
499 [29] D. Takagi, K. Ishizaki, H. Hanawa, T. Mabuchi, G. Shimakawa, H. Yamamoto, C. Miyake,
500 Diversity of strategies for escaping reactive oxygen species production within photosystem I
501 among land plants: P700 oxidation system is prerequisite for alleviating photoinhibition in
502 photosystem I, Physiol. Plant. 161 (2017) 56-74.
503 [30] A. Krieger-Liszkay, G. Shimakawa, P. Sétif, Role of the two PsaE isoforms on O2 reduction
504 at photosystem I in Arabidopsis thaliana, Biochim. Biophys. Acta Bioenerg. 1861 (2020)
505 148089.
506 [31] C. Klughammer, U. Schreiber, An improved method, using saturating light pulses, for the
507 determination of photosystem I quantum yield via $P700^{+}$-absorbance changes at 830 nm, Planta
508 192 (1994) 261-268.
509 [32] P. Sétif, Electron-transfer kinetics in cyanobacterial cells: Methyl viologen is a poor
510 inhibitor of linear electron flow, Biochim. Biophys. Acta Bioenerg. 1847 (2015) 212-222.
511 [33] C. Mignée, R. Mutoh, A. Krieger-Liszkay, G. Kurisu, P. Sétif, Gallium ferredoxin as a tool
512 to study the effects of ferredoxin binding to photosystem I without ferredoxin reduction,
513 Photosynth. Res. 134 (2017) 251-263.
514 [34] M.C.W. Evans, C.K. Sihra, R. Cammack, The properties of the primary electron acceptor
515 in the Photosystem I reaction centre of spinach chloroplasts and its interaction with P700 and
516 the bound ferredoxin in various oxidation-reduction states, Biochem. J. 158 (1976) 71-77.
517 [35] M. Polm, K. Brettel, Secondary pair charge recombination in photosystem I under strongly
518 reducing conditions: temperature dependence and suggested mechanism, Biophysical Journal
519 74 (1998) 3173-3181.
520 [36] A. Tiwari, F. Mamedov, M. Grieco, M. Suorsa, A. Jajoo, S. Styring, M. Tikkanen, E.-M.
521 Aro, Photodamage of iron–sulphur clusters in photosystem I induces non-photochemical energy
522 dissipation, Nat. Plants 2 (2016) 16035.
523 [37] C. Miyake, Molecular mechanism of oxidation of P700 and suppression of ros production

524 in photosystem I in response to electron-sink limitations in C_3 plants, Antioxidants 9 (2020)
525 230.
526 [38] P. Setif, G. Hervo, P. Mathis, Flash-induced absorption changes in Photosystem I, Radical
527 pair or triplet state formation?, Biochim. Biophys. Acta Bioenerg. 638 (1981) 257-267.
528
529
530

Tables

Table 1. Total photo-oxidizable P700 amount (P_m) in cucumber leaves

Treatments	Before	After	Ratio (%)
Continuous light at room temperature	1.39 ± 0.51	1.60 ± 0.48	118 ± 15
Continuous light at low temperature	1.67 ± 0.32	0.93 ± 0.33	55 ± 16
rSP illumination at room temperature	1.44 ± 0.62	0.96 ± 0.54	67 ± 28

Data are represented as the mean ± standard deviation (n = 11, biological replicates).

Table 2. EPR parameters in isolated PSI

Treatments	Spin amounts[a]		Ratio (%)		
	$(F_A\ F_B)_{2red}$	$(F_A\ F_B)_{1red}$	$(F_A\ F_B)_{2red}$ *vs* C/RT	$(F_A\ F_B)_{1red}$ *vs* C/RT	$(F_A\ F_B)_{1red}$ *vs* $(F_A\ F_B)_{2red}$[b]
C/RT	2.25	0.715	100	100	63.5
C/LT	1.57	0.41	70	34	52
F/RT	2.29	0.66	102	92	58

Spin amounts of $(F_A\ F_B)_{2red}$ and $(F_A\ F_B)_{1red}$ were determined in the presence of dithionite at pH 10 and by illumination at pH 8 respectively (see the text for details). PSI preparations used here are those also used for flash-absorption measurements at 800 nm.

[a]Relative units normalized to the same chlorophyll concentration (same OD at red maximum).

[b]For the calculation, spin amounts of $(F_A\ F_B)_{2red}$ were divided by two.

Table 3. Components of flash-induced absorption decay at 800 nm

Treatments	Amplitude (%)			
	Slow phase[a]	Intermediate phase[b]	Fast phase[c]	Slow phase *vs* C/RT
C/RT	100	0	0	100[e] [100][f]
C/LT	67	9 (180)[d]	24 (6)[d]	38[e] [37.5][f]
F/RT	88	8 (530)[d]	4 (10)[d]	47[e] [49][f]

All kinetics result from low intensity (3.1%) 700 nm laser excitation except for a part of the last column[f] (in square brackets). Decay analysis was performed with four exponential components. Data for analysis are those shown in Fig. 2 and Fig. S3.

[a]Slow phases include two components: a first one with $t_{1/2}$ = 16 − 20 ms and a second one with $t_{1/2}$ ≈ 150 − 220 ms, in relative proportions of *ca.* 60/40 for the three different PSIs. These components correspond to PSI containing the terminal acceptor (F_A F_B).

[b]Intermediate phases are attributed to recombination reactions in PSI lacking (F_A F_B) and also possibly F_X.

[c]Fast phases are attributed to the decay of ^{3}P700.

[d]Half time of the decay (µs).

[e]The absorption changes corresponding to these slow phases are 0.576 × 10^{-3}, 0.221 × 10^{-3}, and 0.273 × 10^{-3} for C/RT, C/LT, and F/RT, respectively (after normalization to an OD = 1.7 at red maximum).

[f]Amplitude (%) of slow phases *vs.* C/RT with saturating laser.

535

Table 4. Components of flash-induced absorption decay at 820 nm

Treatments	Amplitude (× 10^{-3})			
	Slow component[a]	^{3}P700 decay[a,b]	Nanosecond decay[a,d]	Initial absorption change[a,e]
C/RT	4.06	0[c]	0[c]	4.06
C/LT	1.54	1.06	0.64	3.24
F/RT	2.21	0	0.24	2.45

All signals analyzed here result from low-intensity (~130 µJ cm^{-2}) 600 nm laser excitations (Fig. 3). The fast decay kinetics measured with C/RT were fitted with three exponential components, and the fitted curve was subtracted from the kinetics of all PSIs (Supplementary Fig. S4). Decay analysis was then performed with two exponential components and an offset level attributed to the slow components. Note that the F/RT sample studied here is significantly different from the one studied at 800 nm and by EPR, as it exhibits a larger microsecond decay attributed to ^{3}P700. The same F/RT sample was used for measuring the ^{3}P700 spectrum in the infrared region (Supplementary Fig. S5).

[a]Data were normalized to an OD = 12 at red maximum.

[b]The triplet decay was fitted with two exponential components with $t_{1/2}$ of 1.4 and 8.1 µs (see Fig. 3).

[c]The value is 0 by construction as the C/RT fast decay kinetics were subtracted from the kinetics of all PSIs.

[d]The decay halftimes were ~50 and ~60 ns for C/LT and F/RT, respectively.

[e]Sum of the initial absorption changes corresponding to slow components, ^{3}P700, and nanosecond decay.

536

Table 5. Amplitudes of double-flash-induced absorption changes at 800 nm

PSI	Signal amplitude[c] ($\times 10^{-3}$)		
	1st flash	2nd flash	Ratio (2nd flash/1st flash)
C/RT[a]	1.140	1.175	1.030
C/LT[a]	0.389	0.434	1.117
F/RT[a]	0.518	0.559	1.079
T. elongatus[b]	1.172	1.209	1.032

Data correspond to Fig. 4.

[a]PSI from cucumber leaves with amplitudes normalized to an OD = 1.70 at the red absorption maximum.

[b]PSI from the cyanobacterium *Thermosynechococcus elongatus*.

[c]The initial amplitudes were obtained from double-exponential fits of the data.

537

538

539

Figure legends

Figure 1: Electron paramagnetic resonance (EPR) spectra of PSI isolated from leaves treated with continuous light at room temperature (C/RT), continuous light at low temperature (C/LT), and repetitive flashes at room temperature (F/RT), respectively. The same samples were studied in A and C on the one hand and in B and D on the other hand. The A/C samples (dithionite) were prepared by freezing under illumination from room temperature down to 200 K whereas the C/D samples (ascorbate) were frozen in darkness. Experimental conditions: (A) under illumination with white light (18000 µmol photons $m^{-2}s^{-1}$), with 5 mM sodium dithionite, 20 µM methyl viologen and 30 µM triquat in 40 mM CAPS buffer at pH 10; temperature, 8 K; microwave power, 20 mW; magnetic field modulation, 2 mT. (B) after 2 minutes illumination with white light at 15 K (18000 µmol photons $m^{-2}s^{-1}$), with 2 mM sodium ascorbate and 30 µM DCPIP in 20 mM Tricine buffer at pH 8.0; light-induced spectra were measured; temperature, 15 K; microwave power, 20 mW; magnetic field modulation, 1 mT. (C) Same samples as in (A) measured in darkness at 25 K; microwave power, 2 mW; magnetic field modulation, 1 mT. (D) Same samples as in (B) and same measurement conditions as in (C). Within each part, all signals are normalized to the same chlorophyll concentrations. Moreover, signal amplitudes are comparable between C and D, where measurements were measured under non-saturating microwave power. Relative spin amounts are given in Table 2.

Figure 2: Flash-absorption kinetics at 800 nm in PSI isolated from leaves treated with continuous light at room temperature (C/RT), continuous light at low temperature (C/LT), and repetitive flashes at room temperature (F/RT), respectively. Experimental conditions: 1 cm cuvettes contained PSI at an optical density (OD) at red maximum of 1.94, 1.75 and 1.70 for C/RT, C/LT and F/RT, respectively; data were normalized to the same OD of 1.70; average of 8 measurements with 700 nm laser flashes of 25 mJ and 0.8 mJ for (A) and (B), respectively; 2 mM sodium ascorbate and 8 µM DCPIP.

Figure 3: Flash-absorption kinetics at 820 nm in PSI isolated from leaves treated with continuous light at room temperature (C/RT), continuous light at low temperature (C/LT), and repetitive flashes at room temperature (F/RT). Experimental conditions: 1 cm cuvettes contained PSI with an optical density (OD) at red maximum of 11.96, 11.74 and 10.61 for C/RT, C/LT and F/RT, respectively; all data were normalized to the same OD of 12; the intensity of the 600 nm laser flash was ca. 0.13 mJ; 4 mM sodium ascorbate and 40 µM DCPIP; Data are

shown on 2 different timescales after subtraction of the C/RT fast decay that was fitted with three exponential components (Supplementary Fig. S5). (A) Data of C/LT and F/RT were fitted with a single exponential decay and a constant (continuous lines), with $t_{1/2}$ of 51 and 58 ns and pre-exponential factors of 0.64×10^{-3} and 0.25×10^{-3} for C/LT and F/RT, respectively. (B) The decay of C/LT was fitted with 2 exponential components (continuous line), with $t_{1/2}$ of 1.4 and 8.1 µs and pre-exponential factors of 0.28×10^{-3} and 0.77×10^{-3}, respectively). Fitting parameters are summarized in Table 4.

Figure 4: Double-flash excitation of PSI. Flash-induced absorption changes were measured at 800 nm on a slow timescale with two 700-nm laser flashes separated by 200 ms. Laser flashes were saturating (signal > 99% with a 50% attenuation) and a control measurement was made with a single flash. Measurements were done C/RT, F/RT, and C/LT PSIs in the presence of 2 mM sodium ascorbate, 8 µM DCPIP and 50 µM methyl viologen with the same samples at those of Fig. 2, except for the addition of methyl viologen. Data were normalized to the same OD of 1.70 at the red maximum. Averages of 8 flashes.

Figure 5: Cofactors of PSI electron transfer and PSI photoinhibition. Shown are the A- and B-branches of PSI with the six chlorophyll molecules (P_{700}: 2 Chl, A_A, A_B, A_{0A}, A_{0B}), two phylloquinones A_{1A} and A_{1B}, the [4Fe-4S] clusters F_x, F_A, and F_B. In F/RT, F_x is damaged, the B-branch remains intact and active while A-branch is inactivated (red circle), leading to 50% full charge separation. In C/LT, 30% of F_AF_B and even more of F_x are damaged, some $^3P700$ is formed likely via charge recombination in the B-branch and charge separation in the A-branch is also inhibited.

Supplementary figures

Fig. S1: Experimental design of photoinhibition treatments.

Fig. S2: Absorption spectra of PSI isolated from leaves treated with continuous light at room temperature (C/RT), continuous light at low temperature (C/LT), and repetitive flashes at room temperature (F/RT). Absorption spectra were normalized to an OD of 1.70 at the red absorption maximum of 678 nm.

Fig. S3: Flash-absorption measurements at 800 nm at varied laser intensities. The samples are those studied in Fig. 2. Same experimental conditions as those of Fig. 2 except the laser intensity

varied from 1.6% (0.4 mJ) to 100% (25 mJ) by using different numbers of 50% neutral density filters. Parts A, B and C correspond to C/RT, C/LT and F/RT PSI, respectively. All data were normalized to the same OD of 1.70 at red absorption maximum. For each PSI, all kinetics were normalized to the same signal size at 10 ms, using the 100% signal as the reference. This allows the saturation properties of the fast µs signals to be compared.

Fig. S4: Identification of the P700 triplet state (^{3}P700) spectrum in PSI treated with continuous light at low temperature (C/LT). C/LT treated PSI (same preparation as the one studied in Fig. 3) was studied by flash-absorption spectroscopy between 730 and 970 nm. Laser excitation was ca. 0.75 mJ at 700 nm, giving about 60% of the maximal extent of charge separation. A global fit with a single exponential component and a constant was performed on all kinetic traces, giving a $t_{1/2}$ = 7.3 µs for the decay. Part A shows a few kinetic traces, at 740, 820 and 870 nm, with fits in continuous lines extrapolated to time zero. Part B: the preexponential factors of the decay phase and the constant values are shown as open red squares and closed black circles, respectively. The red and black spectra exhibit quite different shapes, which are in full agreement with formerly determined (^{3}P700 – P700) and (P700$^+$ – P700) difference spectra, respectively [38].

Fig. S5: Flash-absorption measurements at 820 nm. Kinetics in the presence of 4 mM sodium ascorbate and 40 µM DCPIP were measured at 820 nm with C/RT, C/LT and F/RT PSI on time scales of 80 ms and 300 ns for parts A/C and B/D, respectively. The samples are those studied in Fig. 3 and data were normalized to an $OD_{1\ cm}$ at 12 at red maximum. The 600 nm laser intensity was 2.6 and 0.13 mJ in parts A/B and C/D, respectively. The intensity of 2.6 mJ was quasi-saturating PSI photochemistry, as judged by a decrease of 5% amplitude in the slow decaying component with a 47% intensity (1.25 mJ). The C/RT kinetics at 0.13 mJ laser energy were fitted with 3 exponential components and a constant, with the best fit curve shown in cyan in parts C/D. The fitted curve has the following equation:

$\Delta A \times 10^3 = 1.60 \times e^{-t/0.01042} + 0.13 \times e^{-t/0.4003} + 0.22 \times e^{-t/5.513} + 4.06$ with time in µs (decay kinetics of 10.4 ns, 400 ns and 5.5 µs).

The kinetics shown in Fig. 3 were obtained after subtracting the decaying part of the fitted curve (*i.e.,* without the constant) from all 3 kinetics. This subtraction procedure assumes that the decaying signal is due to antenna signals and that these antenna signals are identical in the 3 types of PSI.

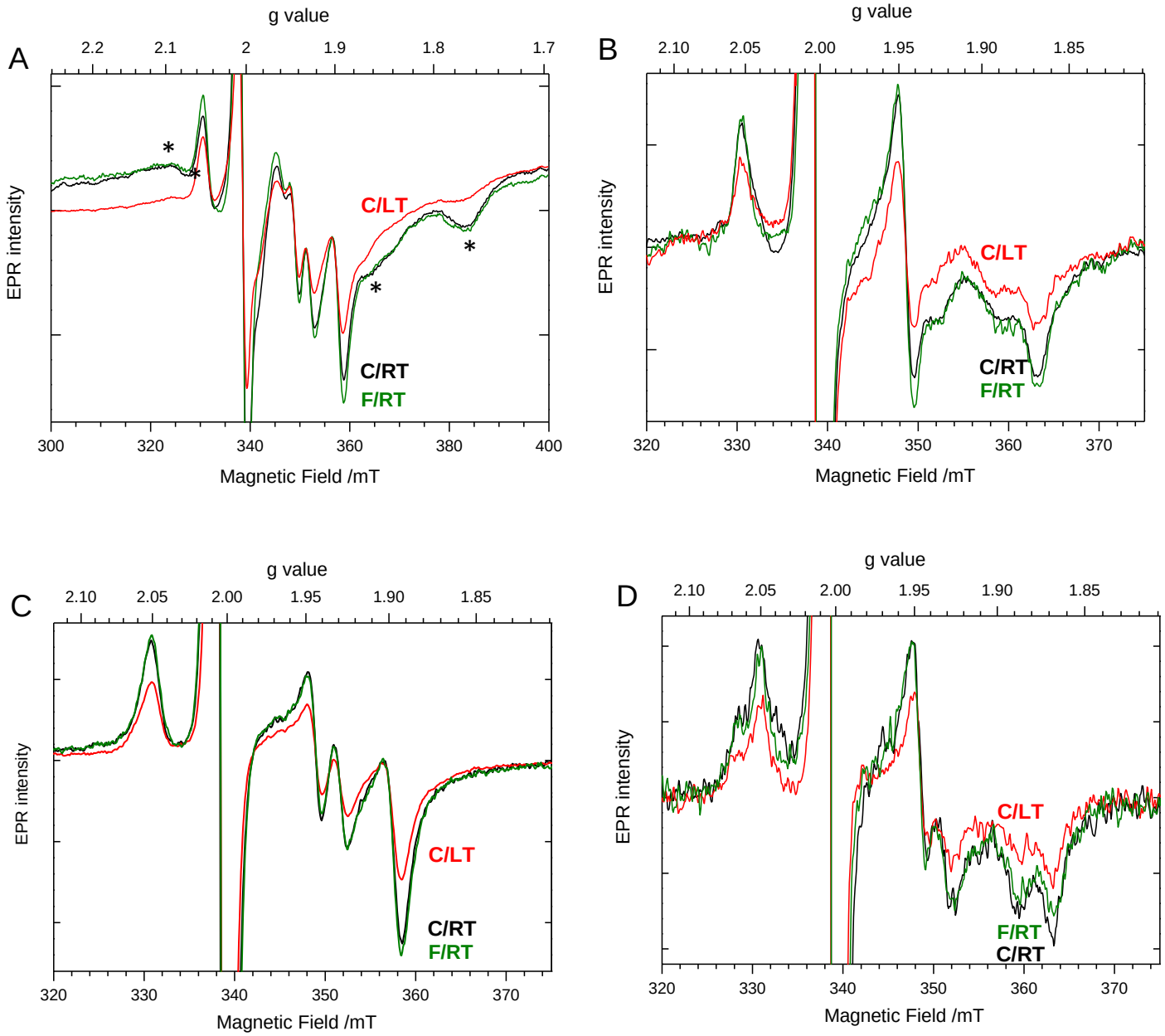
A
g value
2.2
2.1
2
1.9
1.8
1.7
EPR intensity
C/LT
C/RT
F/RT
300
320
340
360
380
400
Magnetic Field /mT
B
g value
2.10
2.05
2.00
1.95
1.90
1.85
EPR intensity
C/LT
C/RT
F/RT
320
330
340
350
360
370
Magnetic Field /mT
C
g value
2.10
2.05
2.00
1.95
1.90
1.85
EPR intensity
C/LT
C/RT
F/RT
320
330
340
350
360
370
Magnetic Field /mT
D
g value
2.10
2.05
2.00
1.95
1.90
1.85
EPR intensity
C/LT
F/RT
C/RT
320
330
340
350
360
370
Magnetic Field /mT

Figure 1

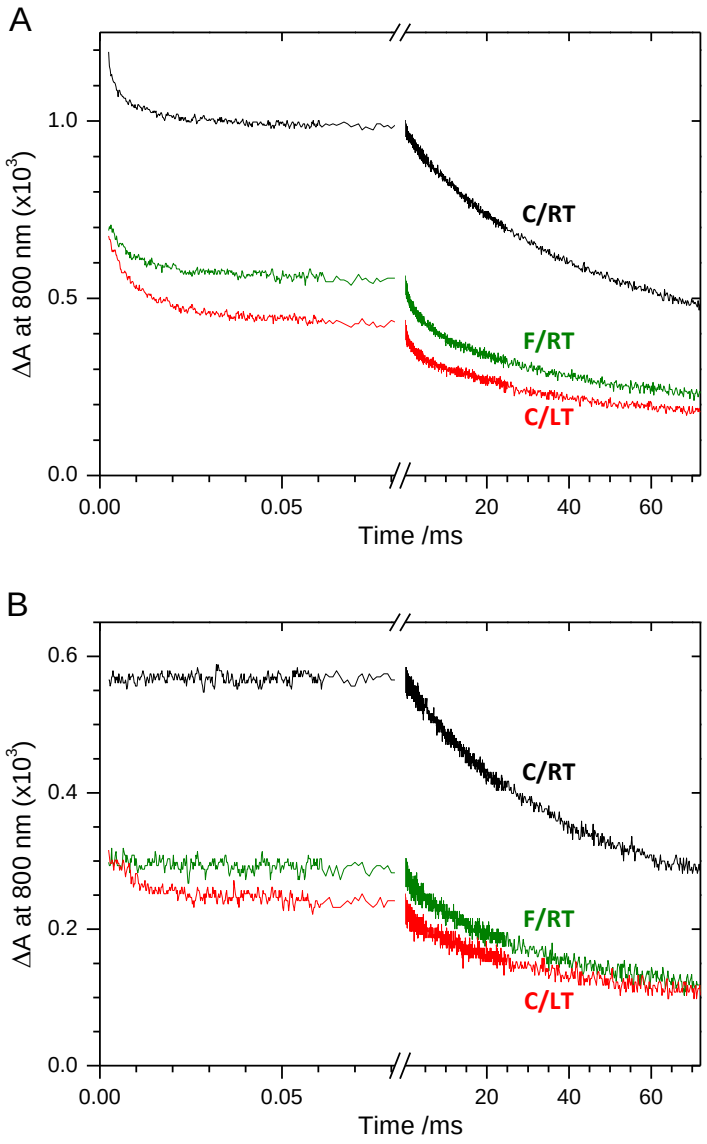
A
1.0
0.5
0.0
ΔA at 800 nm (x10^3)
C/RT
F/RT
C/LT
0.00
0.05
20
40
60
Time /ms
B
0.6
0.4
0.2
0.0
ΔA at 800 nm (x10^3)
C/RT
F/RT
C/LT
0.00
0.05
20
40
60
Time /ms

Figure 2

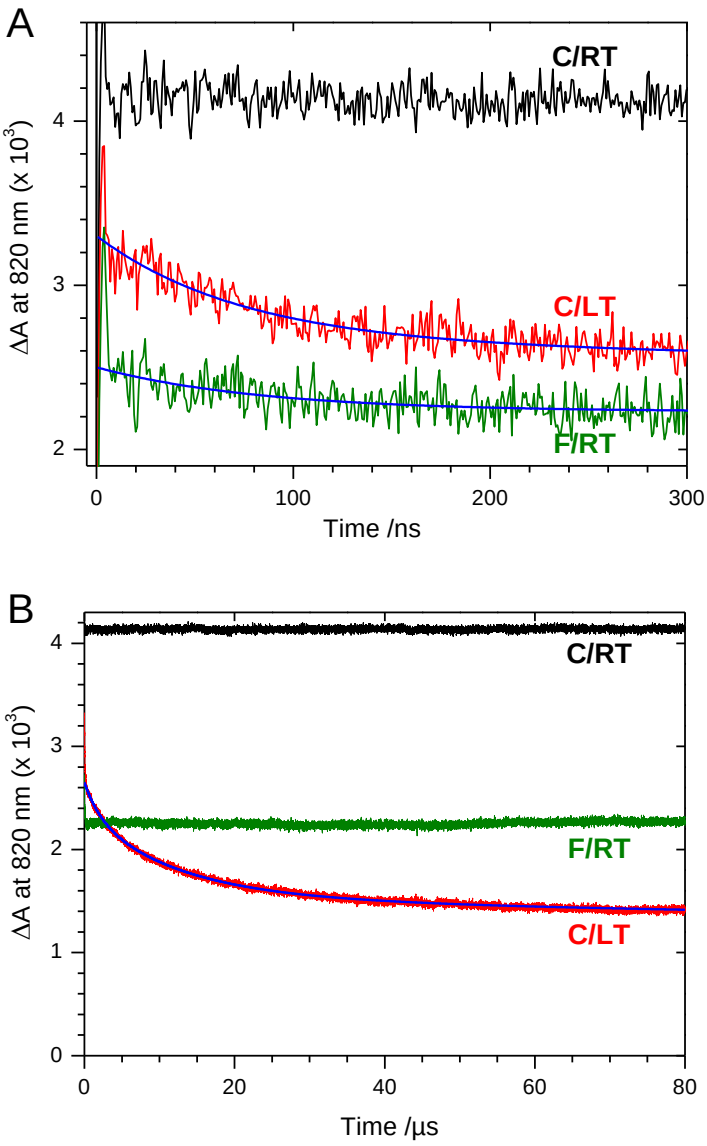
A
C/RT
C/LT
F/RT
ΔA at 820 nm (x 10^3)
Time /ns
B
C/RT
F/RT
C/LT
ΔA at 820 nm (x 10^3)
Time /μs

Figure 3

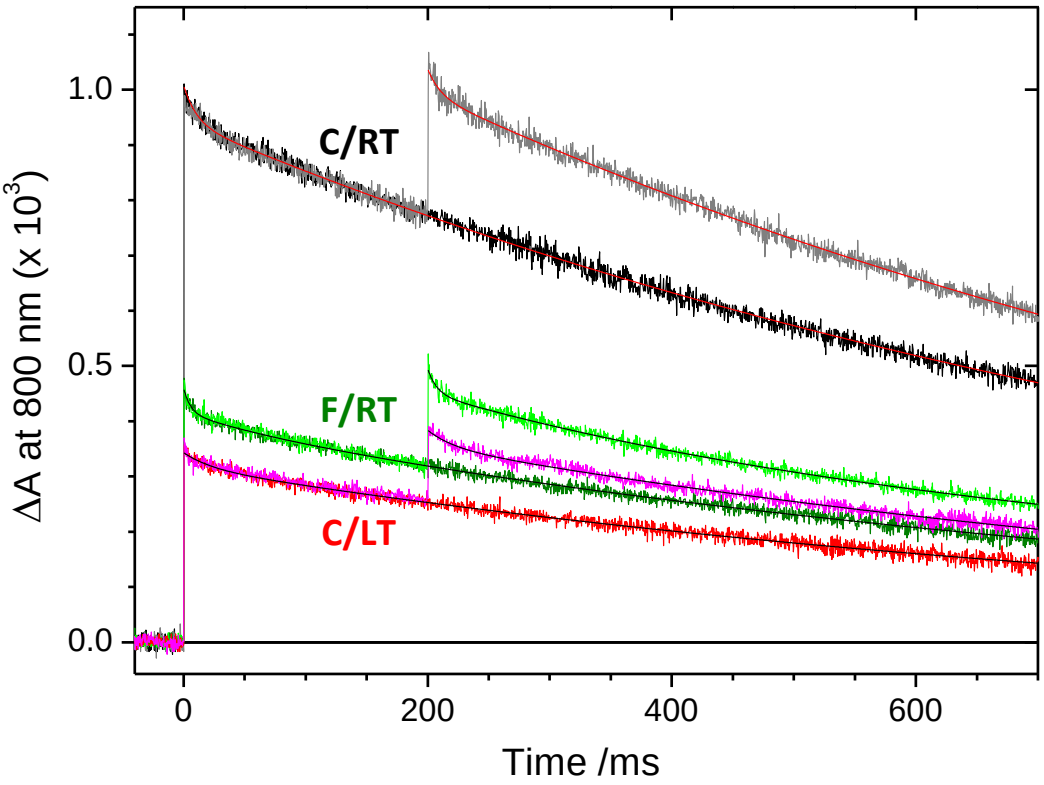

Figure 4

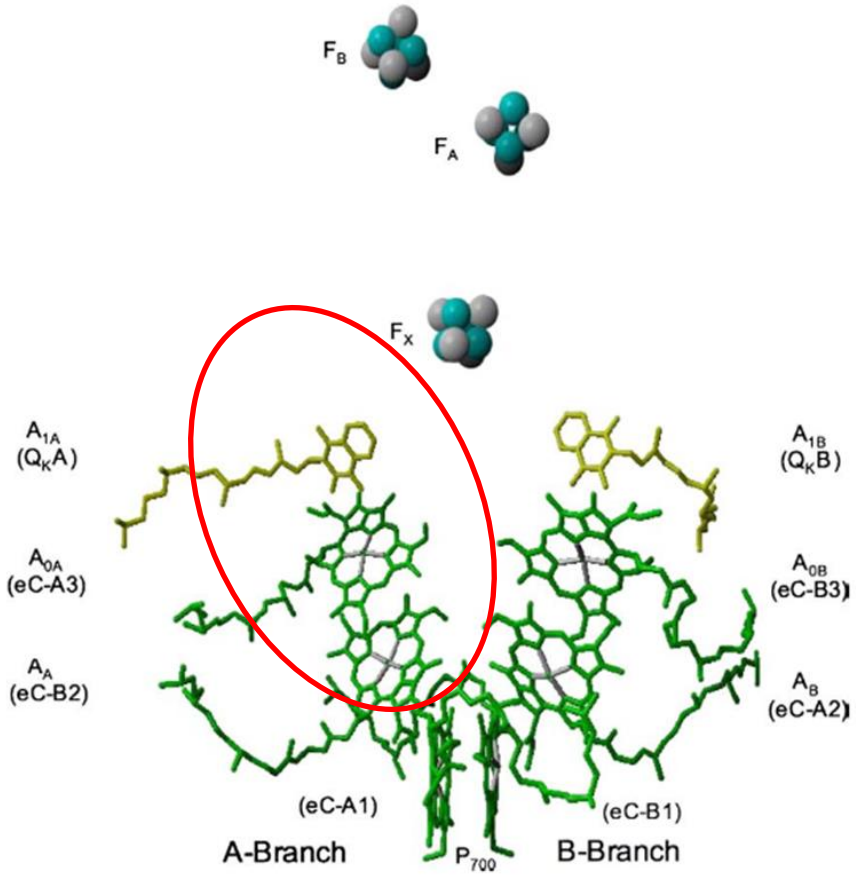
F_B
F_A
F_X
A_1A (Q_K A)
A_0A (eC-A3)
A_A (eC-B2)
A_1B (Q_K B)
A_0B (eC-B3)
A_B (eC-A2)
(eC-A1)
(eC-B1)
A-Branch
P_700
B-Branch

Figure 5